A DFT Study of the Regio- and Stereoselectivity of the 1,3-Dipolar Cycloaddition of C-Methyl Substituted Pyrazinium-3-olates with Methyl Acrylate and Methyl Methacrylate

ARTICLE *in* COMPUTATIONAL AND THEORETICAL CHEMISTRY · DECEMBER 2013

Impact Factor: 1.55 · DOI: 10.1016/j.comptc.2013.09.029

4 AUTHORS:

Lydia Rhyman
University of Mauritius
46 PUBLICATIONS **96** CITATIONS
SEE PROFILE

Ponnadurai Ramasami
University of Mauritius
81 PUBLICATIONS **310** CITATIONS
SEE PROFILE

John A. Joule
The University of Manchester
334 PUBLICATIONS **2,738** CITATIONS
SEE PROFILE

Luis Ramon Domingo
University of Valencia
277 PUBLICATIONS **5,763** CITATIONS
SEE PROFILE

Computational and Theoretical Chemistry 1025 (2013) 58–66

Contents lists available at ScienceDirect

Computational and Theoretical Chemistry

journal homepage: www.elsevier.com/locate/comptc

A density functional theory study of the regio- and stereoselectivity of the 1,3-dipolar cycloaddition of *C*-methyl substituted pyrazinium-3-olates with methyl acrylate and methyl methacrylate

Lydia Rhyman [a], Ponnadurai Ramasami [a,*], John A. Joule [b], Luis R. Domingo [c]

[a] Computational Chemistry Group, Department of Chemistry, University of Mauritius, Réduit, Mauritius
[b] The School of Chemistry, The University of Manchester, Manchester M13 9PL, UK
[c] Departamento de Química Orgánica, Universidad de Valencia, Dr. Moliner 50, 46100 Burjassot, Valencia, Spain

ARTICLE INFO

Article history:
Received 24 July 2013
Received in revised form 27 September 2013
Accepted 27 September 2013
Available online 8 October 2013

Keywords:
1,3-Dipolar cycloaddition
Pyrazinium-3-olate
Methyl acrylate
Methyl methacrylate
Skeleton rearrangement

ABSTRACT

A DFT [B3LYP/6-31G(d)] study was carried out on the 1,3-dipolar cycloaddition (13DC) reactions of multi C-methyl substituted pyrazinium-3-olates with methyl acrylate (MA) and methyl methacrylate (MMA). Thermodynamic and kinetic parameters of the possible *endo*/*exo* stereoisomeric and 6-ester/7-ester regioisomeric pathways have been determined. The skeleton rearrangement of the 6-*exo* [3 + 2] cycloadducts into the [4 + 2] adducts is also considered. The electrophilic, P_k^+, and nucleophilic, P_k^-, Parr functions are used to have better understanding of the regioselectivity of these 13DC reactions. In all cases the *exo* pathways are more favourable compared to the *endo* alternatives. Inclusion of methyl groups at the C-2 and C-5 positions of pyrazinium-3-olate shows that the 7-*exo* cycloadduct is predicted to be the major product followed by its 6-*exo* isomer. These theoretical results have been compared with the previously reported studies on 13DCs of unsubstituted and substituted pyrazinium-3-olates with MA and MMA. The activation energy of these 13DCs ranges from 42.5 to 98.2 kJ mol^{-1} in THF.

1. Introduction

Cycloaddition reactions play a pivotal role in organic synthesis and mechanistic studies [1]. The 1,3-dipolar cycloaddition (13DC) reaction, which is the union of a 1,3-dipole with a dipolarophile, is an effective route for the synthesis of five-membered heterocyclic structures [2,3] as displayed in Scheme 1. 13DC reactions have traditionally been studied by using the frontier molecular orbital (FMO) theory and transition state theory (TST), until recently the reactivity indices, as defined by the conceptual density functional theory (DFT) [4], have been used to rationalise the reactivity and regiochemistry of cycloaddition reactions. Recently, Domingo and coworkers [5] proposed electrophilic, P_k^+, and nucleophilic, P_k^-, Parr functions, based on the atomic spin density distribution in the radical anion and radical cation of the neutral molecules, to study the regioselectivity in polar reactions.

13DCs of pyridinium-3-olates and pyrazinium-3-olates with methyl acrylate (MA, **2**) were studied theoretically by the B3LYP/6-31G(d) method [6,7] (see Schemes S1 and S2 in Supplementary Information (SI)) and our findings were in accord with experimental outcomes [8–11], showing that the regioisomeric 6-ester cycloadducts (CAs) (for numbering see Scheme 2) are formed preferentially. In enlarging the range of *C*-substituted pyrazinium-3-olates, we extended our theoretical studies by assessing the influence of introducing *C*-methyl substituents on the pyrazinium-3-olate ring [7,12] (see Scheme S2 in SI). Again, it was found that the formation of 6-esters is preferred over the 7-esters and the channel leading to the 6-*exo* CA was found to be dominant. However, we revealed that the introduction of a methyl group at C2 of the 1,3-dipole favours the formation of the 7-*exo* CA in contrast to the other substituted pyrazinium-3-olates.

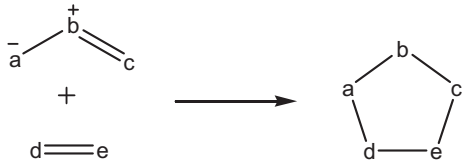

Scheme 1. 13DC reaction.

Following on and inspired by the experimental [13–16] and theoretical results [12,17], the 13DCs of a more hindered alkene, methyl methacrylate (MMA, **3**), with pyridinium-3-olates and pyrazinium-3-olates were also studied. Here again, the reaction channels leading to the formation of the 6-*exo* CAs are the dominant ones followed by the formation of the 7-*exo* and 6-*endo* CAs, except

* Corresponding author.
E-mail address: ramchemi@intnet.mu (P. Ramasami).

2210-271X/$ - see front matter © 2013 Elsevier B.V. All rights reserved.
http://dx.doi.org/10.1016/j.comptc.2013.09.029

for the 13DC of 1,2-dimethylpyrazinium-3-olate where the activation energies increase in the order 7-*exo* < 6-*exo* < 6-*endo* < 7-*endo*.

Within the context of our ongoing work in the reaction mechanism, we looked into [17] the cycloaddition reaction of 1,5,6-trimethyl pyrazinium-3-olate (**1a**, Scheme 2) with MMA **3** where a more complex lactone–lactam structure was obtained experimentally and characterised by X-ray crystallography [16]. However, our theoretical results showed that the formation of the lactone–lactam is a domino process [17]. Further, an intramolecular interaction between the ester carbonyl group oxygen and the iminium cation to produce the five-membered lactone, after rearrangement into its corresponding [4+2] CA, which was observed experimentally, is only present in the CA6ex-1a, thus generating the lactone–lactam [17]. In view of the previous studies [6,7,12,17], the objectives of this work have been twofold: (1) to examine the effect on 13DCs of having more methyl groups on the pyrazinium-3-olates and (2) to investigate the possible rearrangement of the 6-*exo* CA as summarised in Scheme 2. The results obtained are critically analysed and compared with our previously reported theoretical outcomes [6,7,12,17] on 13DCs of unsubstituted and substituted pyrazinium-3-olates **1a–d** with both MA **2** and MMA **3**. The findings from this research and our previous observations complete a systematic investigation of the inclusion of methyl groups at various positions on the pyrazinium-3-olate ring and possible rearrangement of the [3+2] 6-*exo* CA.

2. Computational methods

Full geometry optimisations were carried out for the reactants, TSs and CAs using the DFT with the B3LYP [18,19] functional and the 6-31G(d) [20] basis set. Previous work has shown that the B3LYP/6-31G(d) level is widely used and considered to be reasonable accurate for the activation energies of cycloaddition reactions, although the reaction exothermicities are underestimated by about 5 kcal/mol [21,22]. Vibrational frequencies were computed to establish the nature of stationary points and each TS gave one negative eigenvalue corresponding to the motion involving the formation of the newly forming C–C bonds. The vibrational mode was assigned appropriately by means if visual inspection and animation using the CYLview software [23]. Solvent effects of THF ($\varepsilon = 7.43$) were taken into account with the polarizable continuum model (PCM) as developed by Tomasi's group [24–26] in the framework of self-consistent reaction field (SCRF) [27,28]. The reported thermodynamic data include zero point energy (ZPE) corrections and are given at 298.15 K. The harmonic vibrational frequencies were scaled by a factor of 0.96 [29]. Intrinsic reaction coordinate (IRC) [30] computations starting at the saddle points were carried out to check the connections between the TSs and the reactants and CAs using the second order González–Schlegel integration method [31,32]. Natural bond orbital (NBO) analysis was also accomplished on the electronic structures of the critical points according to Weinhold and coworkers [33,34]. All the computations were performed using the Gaussian 09 suite of programs [35].

The global electrophilicity index, ω, was calculated following the expression [36–39], $\omega\,(\mu^2/2\eta)$, where μ is the electronic chemical potential, $\mu \approx (\varepsilon_H + \varepsilon_L)/2$, and η is the chemical hardness, $\eta \approx (\varepsilon_L - \varepsilon_H)$. The nucleophilicity index, N [37], which we have recently introduced is defined as $N = \varepsilon_{H(Nu)} - \varepsilon_{H(TCE)}$, where tetracyanoethylene (TCE) is chosen as the reference. This choice allowed us conveniently to handle a nucleophilicity scale of positive values [40,41]. The local electrophilicity indices [42], ω_k, and the local nucleophilicity indices [43], N_k, were evaluated using the following expressions:[24] $\omega_k = \omega P_k^+$ and $N_k = NP_k^-$, where P_k^+ and P_k^- are the electrophilic and nucleophilic Parr functions, respectively, obtained through the analysis of the Mulliken atomic spin density of the radical anion and the radical cation [5].

3. Results and discussion

3.1. Energetics

These 13DCs follow a one-step mechanism and proceed to give the *exo* and *endo* CAs from the two possible regiochemical pathways (Scheme 2). The four TSs, designated **TS6en-1x**, **TS6ex-1x**, **TS7en-1x**, **TS7ex-1x** and the corresponding CAs, **CA6en-1x**, **CA6ex-1x**, **CA7en-1x**, **CA7ex-1x**, where **x** (**x** = **a, b, c** and **d**) denotes the substituted pyrazinium-3-olates taken into consideration, were located and characterised. Similarly for the skeleton rearrangement, the TSs were labeled as **TS6en-1x-2**, **TS6ex-1x-2**, **TS7en-1x-2**, **TS7ex-1x-2** and their corresponding CAs, **CA6en-1x-2**, **CA6ex-1x-2**, **CA7en-1x-2**, **CA7ex-1x-2** were located.

The calculated relative energies of the 13DCs of **1a–d** with MA **2** and MMA **3** in both the gas phase and in THF as solvent are gathered in Table 1 (more details available as SI, in Tables S1–S4).

Analysis of the gas phase activation energy data from Table 1 shows that the *exo* approaches are favoured over the *endo* isomers, and the relative energies for the reaction with MMA **3** are higher compared to the relative energies for the reactions with MA **2**. The computed gas phase relative energies are not consistent with

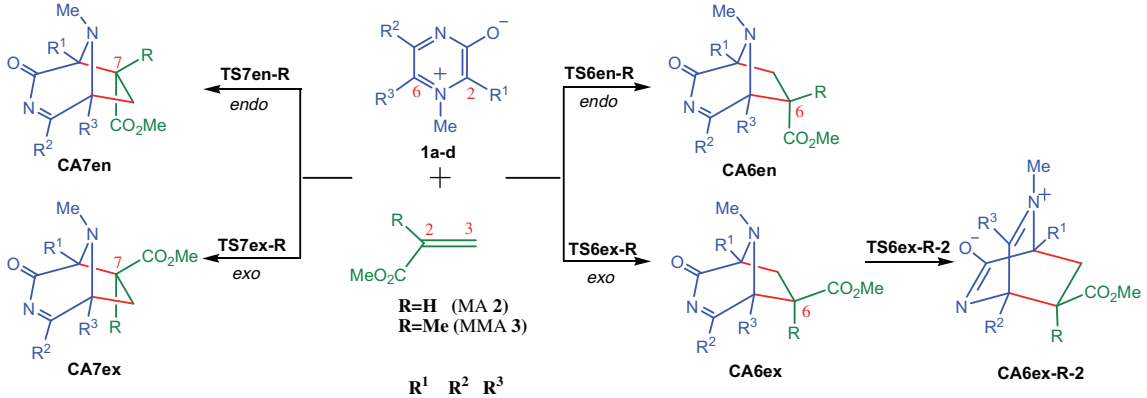

	R^1	R^2	R^3
1a	H	Me	Me (**CA6ex** was observed as the major product [14])
1b	Me	Me	H
1c	Me	H	Me
1d	Me	Me	Me

Scheme 2. Model substrates for the 13DC of *C*-methyl substituted pyrazinium-3-olates (**1a–d**) with MA **2** and MMA **3**.

Table 1
Relative energies[a] (ΔE, in kJ mol^{-1}) in gas phase and THF involved in the 13DC reactions of **1a–d** with MA **2** and MMA **3**.

	MA **2**				MMA **3**			
	1a	**1b**	**1c**	**1d**	**1a**	**1b**	**1c**	**1d**
Gas phase								
TS6en	50.7	63.0	61.1	57.0	66.9	73.3	77.9	66.8
TS6ex	25.8	42.5	37.2	33.1	35.6	64.2	46.5	54.9
TS7en	60.2	59.5	65.6	59.3	82.6	69.5	88.9	71.8
TS7ex	45.7	41.5	48.7	42.4	56.4	59.3	58.6	61.7
CA6en	−68.9	−58.0	−52.9	−64.5	−42.4	−29.2	−30.0	−34.8
CA6ex	−68.3	−62.8	−51.1	−63.6	−38.5	−34.3	−25.4	−34.6
CA7en	−73.1	−60.7	−54.5	−67.8	−56.5	−31.6	−28.5	−38.0
CA7ex	−46.7	−56.7	−51.9	−64.4	−57.5	−28.9	−25.2	−34.9
THF								
TS6en	60.3	73.3	70.8	74.9	70.8	87.2	82.7	79.7
TS6ex	48.5	64.2	59.0	44.5	55.3	72.9	56.9	63.5
TS7en	74.2	69.5	78.9	81.4	93.6	86.4	98.2	90.3
TS7ex	67.4	59.3	69.7	51.8	74.5	65.9	76.8	68.8
CA6en	−36.3	−29.2	−21.6	−37.1	−13.4	−15.9	−0.9	−11.0
CA6ex	−36.6	−34.3	−19.8	−33.9	−10.3	−18.0	2.3	−8.7
CA7en	−40.2	−31.6	−22.6	−41.6	−26.9	−9.0	0.7	−15.0
CA7ex	−42.3	−28.9	−19.9	−34.9	−27.9	−7.0	3.0	−12.5

[a] Relative to **1x** (**x** = **a**, **b**, **c**, **d**) + MA **2**/MMA **3**.

the experimental regioselectivity reported in the literature [14] for the reaction of **1a** with MA **2**, thus in the following, only the results obtained in THF are taken into account, as the reported theoretical findings compare satisfactorily with the experimental outcomes. In THF, the reactants are slightly more stabilised than the TSs and this results in an increase in the activation energies as the zwiterionic 1,3-dipoles are more polar than the TSs [44]. Generally, the **TS6ex** is kinetically favoured except for the reaction of **1b** with MA **2** and MMA **3** where **TS7ex** has lower activation energy than **TS6ex**.

The *exo* pathways have lower activation energy compared to the *endo* pathways and this can be explained in terms of the partially negative ester carbonyl oxygen in the *exo* TSs which is closer in space to the partially positive nitrogen, N1. Thus, considering the C2–N1–C6 framework of these pyridinium-3-olates as the allylic-type 1,3-dipole, these 13DCs are "*endo*"-selective.

In contrast to the various studied systems, for the reactions of **1a** with both MA **2** and MMA **3**, it is found that the 6-esters are kinetically preferred over the 7-esters; the energy differences between the 6-esters are 11.8 and 15.5 kJ mol^{-1} with MA **2** and MMA **3**, respectively. On comparing these theoretical data with our previous computations, we found that the inclusion of a methyl group at C-6 of the pyrazinium-3-olate always leads to formation of 6-esters, whichever dipolarophile used.

From kinetic and thermodynamic points of view, the energetic results show that the most preferred pathway is the one leading to the **CA6ex** except for the reaction of **1b** with MA **2** and MMA **3** where the predominating CA is 7-*exo*. The expected CAs for the reaction of **1a** with both MA **2** and MMA **3**, would be the 6-ester CAs with the 6-exo CA as the major product followed by the 6-*endo* CAs. We found that the inclusion of a methyl group at C-5 and C-6 positions yielded the 6-ester CAs with both MA **2** and MMA **3**. Therefore, we can conclude that the presence of a methyl group at the C-6 position of the pyrazinium-3-olate favours the 6-ester reaction channels.

The 13DC of **1b** with MA **2** shows that the relative energy of the 7-*exo* channel is comparable to that of the 6-*exo* channel, the energy difference between the 6-*exo* and the 7-*exo* channels being 4.9 kJ mol^{-1} in THF. Therefore, the major product is predicted to be the 7-*exo* CA followed by a mixture of 6-*exo* and 7-*endo* CAs as the energy difference between these two reaction pathways is 5.3 kJ mol^{-1}. It is noteworthy that reaction of **1b** with MA **2** is the only one where a minor amount of 7-*endo* CA was isolated experimentally. A similar observation was made for the reaction of **1b** with MMA **3**, and here the theoretical results suggest that the reaction mixture would have 6-*exo* only as a minor product and 7-*exo* as the predominating CA (the energy difference between the 6-*exo* and 7-*exo* TSs is 7.0 kJ mol^{-1}) as the 7-*endo* reaction pathway has a higher activation energy (86.4 kJ mol^{-1}). Likewise, the reaction of 1,2-dimethylpyrazinium-3-olate with MA **2** and MMA **3**, as previously reported [7,12], favoured the 6-*exo* and 7-*exo* pathways. Therefore, the absence of a substituent (methyl) at C-6 of the pyrazinium-3-olate encourages the formation of a 7-*exo* CA.

An explanation for the formation of 7-CAs when the pyrazinium-3-olate C-2 carries a methyl and C-6 is unsubstituted could involve steric or electronic factors, or both. In an attempt to study the formation of 7-CAs, the 13DCs of MA **2** and MMA **3** with 1-methylpyrazinium-3-olates were studied by varying the substituent at the C-2 position, changing it into an ethyl or a bulky *t*-butyl group. The results are listed in Table S5 in SI. Our computations show that 7-*exo* CAs are predicted, in each case, despite the changes in C2-substitutent size. Thus, the preference for 7-CAs from 6-unsubstituted pyrazinium-3-olates is not influenced or altered by the size of the C2-substituent. An analysis of the reaction between the most hindered pyridinium-3-olate (i.e. with a 2-*t*-butyl group) with the more hindered MMA **3**, indicates that there is a return to the 6-*exo* pathway, being slightly preferred kinetically over the 7-*exo* pathway (4.0 kJ mol^{-1}).

Considering the polarisation of the pyrazinium-3-olates and the effect that alkyl (electron donating) groups have, we can see that a 6-alkyl substituent will decrease electron density at C6 and thus decrease the tendency for C6 to interact nucleophilically with the acrylate (necessary for formation of a 7-ester). The converse is that with no substituent at C-6, the tendency for the initial interaction with the acrylate to involve C6 as a nucleophile will be increased, thus leading to a 7-ester. These effects will be exaggerated by electron-donating (alkyl) groups at C2 which will decrease electron density at C2, i.e. decrease the tendency for C2 to interact nucleophilically with the acrylate (necessary for formation of the 6 esters). These arguments are summarised in Scheme 3.

It can be predicted that, for the reaction of **1c** and **d** with MA **2** and MMA **3**, a mixture of the *exo* CAs with a predominating 6-*exo* CA would result. However, the reaction of **1c** with MMA **3** is endothermic as observed for the reaction of 1,2-dimethylpyrazinium-3-olate with MMA **3** [12]. This is because the polar solvent increases the activation energy and thus, makes the reaction less exothermic [44].

Activation parameters, namely, enthalpies, Gibbs energies and entropies for the 13DCs at 298.15 K and 1 atm are summarised in Table S6 in SI. Inclusion of thermal corrections and entropies in the electronic energies increases the Gibbs energies, and thus, these 13DCs become endergonic. The activation enthalpy shows a preference for the *exo* approach in agreement with the predicted activation energy. In addition, the activation entropy corresponding to the *exo* approach is more negative than that corresponding to the *endo* approach. As a consequence, the activation Gibbs energy for formation of the **CA6ex** and **CA7ex** is lower than that for the **CA6en** and **CA7en**.

3.1.1. Effects of the methyl substitution on the reactions of methyl-substituted pyrazinium-3-olates and dipolarophiles

On comparing the 13DCs of unsubstituted and N1 and C-methyl substituted pyrazinium-3-olates with MA **2** and MMA **3** (see Figs. 1 and S1–S3 in SI), it is found that the activation energies for their reactions with MMA **3** are always higher than with MA **2** except for the 6-*exo* reaction pathway of (**1c**), in which the C-2 and C-6

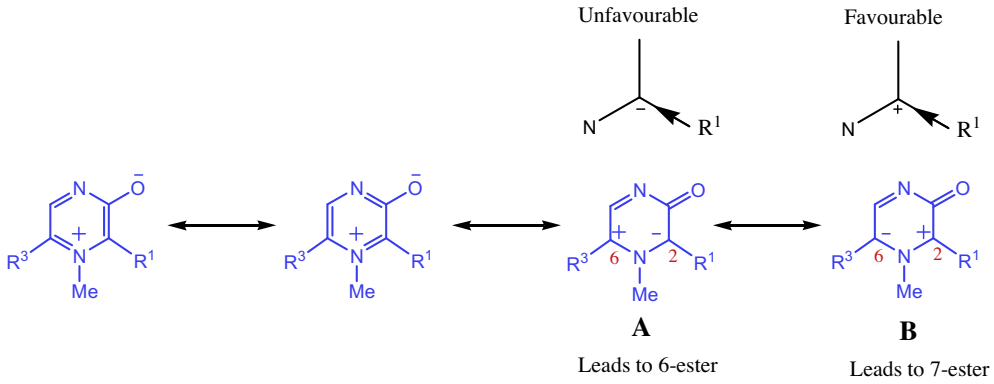

Resonance contributor **B** is less important if R^3 is electron-donating (i.e. not H) and resonance contributor **A** is more important if R^3 is electron-donating (i.e. alkyl)

Scheme 3. Resonance contribution based on R^3 of the pyrazinium-3-olates.

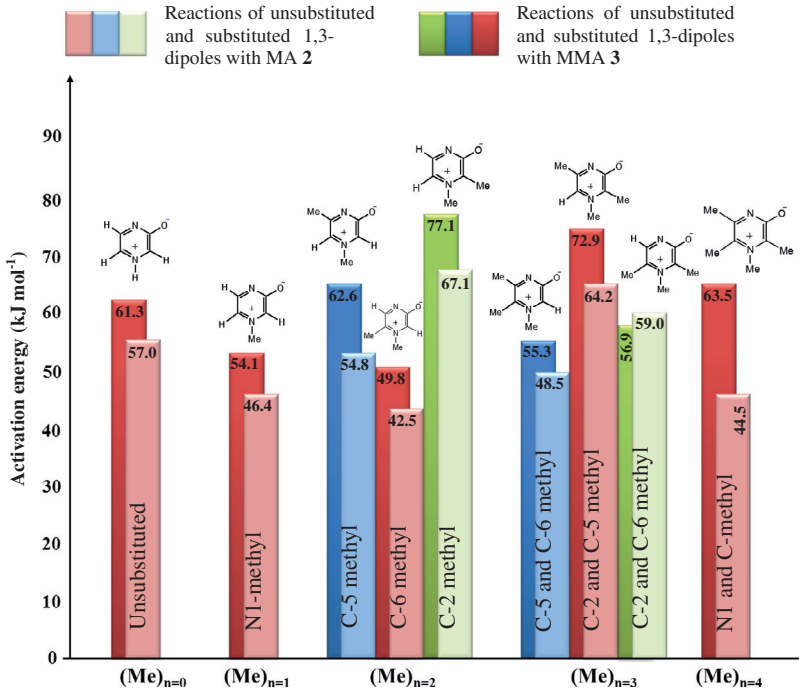

Fig. 1. Calculated activation energy of the 6-*exo* reaction pathway of unsubstituted and substituted pyrazinium-3-olates with MA **2** and MMA **3**. (For all $(Me)_{n=2,3}$, the N1 of the pyrazinium-3-olate is substituted by methyl).

of the pyrazinium-3-olates are substituted by methyl groups, with an activation energy difference of 2.1 kJ mol^{-1}. The difference in activation energy between the reactions with MA **2** and MMA **3** are in the range 4.3–22.0 kJ mol^{-1}. This behaviour can be interpreted as a decrease of the electrophilic character of MMA **3** with the presence of the electron-releasing methyl group at the C2 position (see Section 3.4).

On considering the unsubstituted, and the all C-methyl substituted, pyrazinium-3-olates, it is found that the reactions of all the C-methyl substituted pyrazinium-3-olates with MMA **3** have higher activation energies than reactions with the unsubstituted pyrazinium-3-olate for the 6-*endo* and 6-*exo* pathways; 3.8 and 2.2 kJ mol^{-1}, respectively. However, for the 7-*endo* and 7-*exo* pathways, the activation energies for the reaction of unsubstituted pyrazinium-3-olate with MMA **3** are slightly higher than its reaction with the all C-methyl substituted pyrazinium-3-olates by 1.9 and 2.2 kJ mol^{-1}, respectively. Moreover, for the 6-*endo* and 7-*endo* pathways, the reactions of all the C-methyl substituted pyrazinium-3-olates with MA **2** have higher activation energies than the reactions of unsubstituted pyrazinium-3-olate with MA **2**, by 6.8 and 4.3 kJ mol^{-1}, respectively. On the other hand, reaction of all the C-methyl substituted pyrazinium-3-olates with MA **2** have lower activation energies by 12.5 and 14.4 kJ mol^{-1}, for the 6-*exo* and 7-*exo* reaction pathways, respectively.

In general, the activation energy increases in the following order: 6-*exo* < 7-*exo* < 6-*endo* < 7-*endo*. For the most favourable pathway, the 13DC reactions of N-1 and C-6 methyl substituted pyrazinium-3-olates with both MA **2** and MMA **3** have lowest activation energy of 42.5 kJ mol^{-1} (Fig. 1, [7,12]). It is noteworthy that when the pyrazinium-3-olate is substituted at the C-2 position, its reaction with MA **2** and MMA **3** proceeds *via* high activation energy whereas reactions of C-5 and C-6 methyl substituted pyrazinium-3-olates have lower activation energy. In addition, the C-6-methyl substituted pyrazinium-3-olate presents the lowest activation

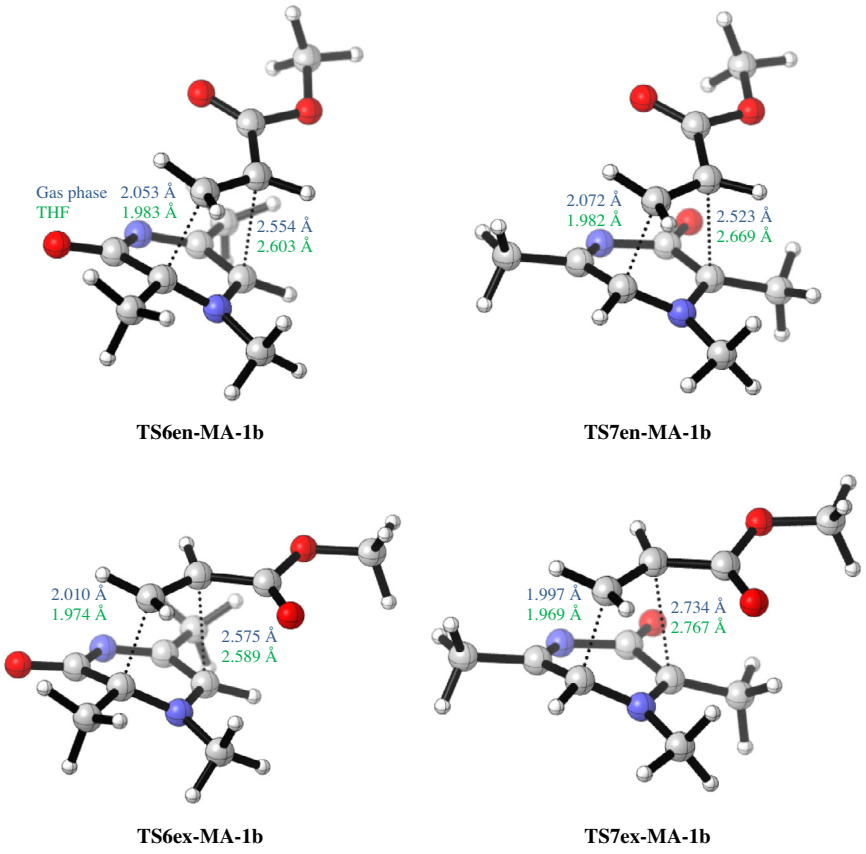

Fig. 2. B3LYP/6-31G(d) optimised geometries of the TSs involved in the 13DC between **1b** with MA **2**.

energy as this has the least steric congestion and the best partial charge stabilization.

*3.1.2. Skeleton rearrangement of the [3+2] CAs **CA6ex** into the [4+2] CAs **CA6ex-2***

Based on our recent investigation [17], we also studied the conversion of the [3+2] CA into the [4+2] CA for the 6-*exo* CAs only for the reactions of **1a**–**d** with both MA **2** and MMA **3** (Figs. S10 and S11 in SI). The energetic results are collected in Tables S7 in SI. The reactions have been studied in THF and acetonitrile for comparison purposes [17]. The results indicate that the rearrangement processes, within the margin of error, are feasible in acetonitrile with both MA **2** and MMA **3** dipolarophiles although the [4+2] CAs are not thermodynamically stable compared to the [3+2] CAs. Additionally, these rearrangements are kinetically favourable in THF whereas the formation of the corresponding [4+2] CAs are thermodynamically unfavourable.

3.2. Geometrical parameters

The geometries of the TSs involved in the 13DCs of the pyrazinium-3-olates with MA **2** and MMA **3** are presented in Figs. 2 and 3, and Figs. S4-S9 in SI. An analysis of the lengths of the two σ forming bonds at the TSs associated with these 13DCs indicates that the reactions involve asynchronous bond-formation processes. At the regioisomeric TSs, the lengths of the C3–C2 and C3–C6 forming bonds are shorter than the C2–C6 and C2–C2 bonds, respectively. Consequently, the C–C bond formation at the more electrophilic conjugated C3 position of MA **2** and MMA **3** is more advanced than that at C2 and the addition of a methyl group on the dipolarophile causes an increase in the bond lengths between the substituted pyrazinium-3-olates and MMA **3**.

The asynchronicity of bond formation at the TSs is measured by considering the difference between the lengths of the two σ forming bonds such that Δd_6 = [d(C2–C6) – d(C3–C2)] for 6-ester pathways and Δd_7 = [d(C2–C2) – d(C3–C6)] for 7-ester pathways. Table 2 reports the degree of asynchronicity, Δd, leading to the TSs in THF. The 13DCs of **1a**–**d** with MMA **3** are more asynchronous compared to the reactions of **1a**–**d** with MA **2**. Thus, we can conclude that the presence of methyl groups leads to more asynchronous 13-DCs. Overall there are varying degrees of asynchronicity but generally, the trend is that formation of the *exo* TSs is consistently more asynchronous relative to formation of the *endo* TSs.

The greater Δd for MMA **3** than for MA **2** can be understood as a hindrance between the methyl group present at C2 of MMA **3** and the substituents present in pyrazinium-3-olate ring. The greater Δd can be also electronically explained by the presence of the electron-releasing Me at C2 carbon, which polarises the electron-density towards C1 carbon. Note that these highly asynchronous TSs are associated to a two-centre interaction in which only the σ bond at the C2 conjugated position of MA **2** and MMA **3** is being formed; the force constant associated with the formation of the second σ bond being very weak. Consequently, any electronic or steric interaction can modify this distance, changing the Δd at the TSs.

We can also conclude that the Δd of **1a** and **1b** are comparable with the 1,2-dimethylpyrazinium-3-olate and 1,6-dimethylpyrazinium-3-olate [7,12]. The Δd of **1c** roughly corresponds to the median of the Δd of **1a** and **1b** as displayed in Fig. 3. The Δd of **1d** is also comparable to that of **1c** (see Fig. 4).

3.3. Bond order and charge analysis

The nature of the TSs was examined using the Wiberg bond indices [45]. Table 3 shows the bond order (BO) values of the

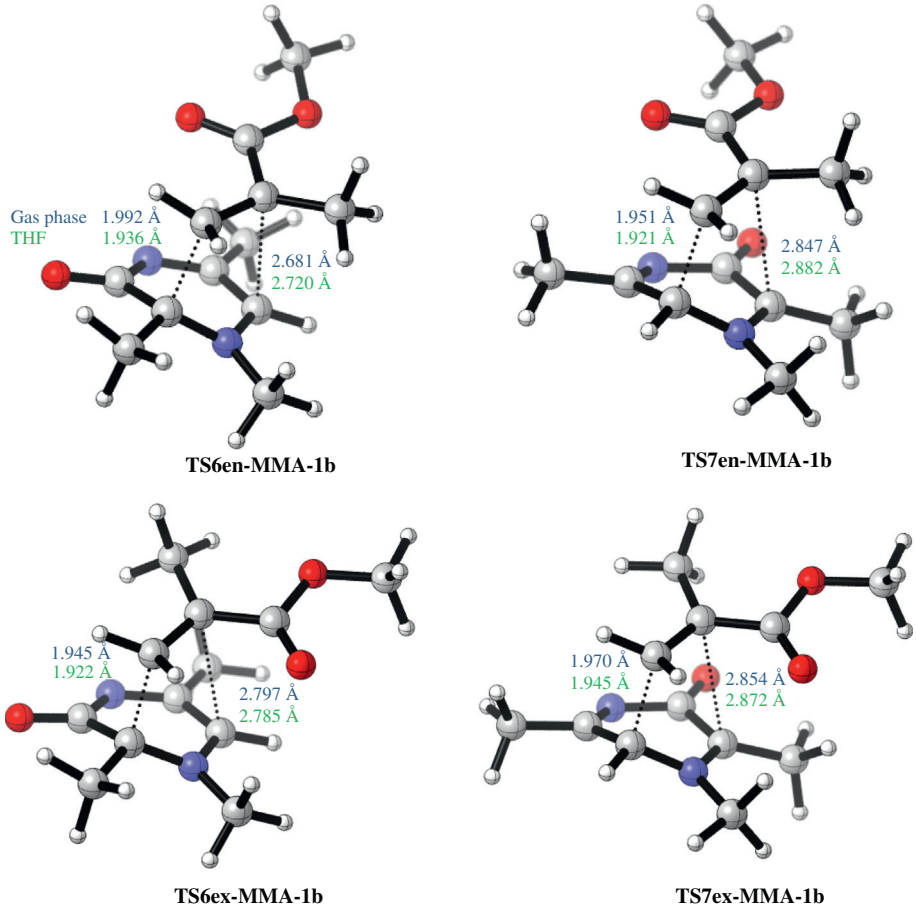

Fig. 3. B3LYP/6-31G(d) optimised geometries of the TSs involved in the 13DC between **1b** with MMA **3**.

Table 2
Δd at the TSs arising from the 13DCs of **1a–d** with MA **2** and MMA **3**.

	1a	1b	1c	1d
MA **2**				
TS6en	0.77	0.62	0.69	0.66
TS6ex	0.77	0.62	0.72	0.70
TS7en	0.39	0.69	0.48	0.54
TS7ex	0.53	0.80	0.71	0.68
MMA **3**				
TS6en	0.88	0.78	0.86	0.83
TS6ex	1.01	0.86	0.92	0.90
TS7en	0.61	0.96	0.83	0.80
TS7ex	0.75	0.93	0.93	0.84

two C–C forming bonds at the TSs for the 13DCs of **1a–d** with MA **2** and MMA **3**, respectively. For the two possible regioisomeric pathways, the BOs for the forming C3–C2 and C3–C6 bonds have larger values that the C2–C6 and C2–C2 bonds respectively, showing asynchronicity along the bond formation process. These BO data are in agreement with the predicted degree of asynchronicity. Note that in both 13DCs, the bond formation at the conjugated C3 position of MMA **3** is more advanced than that at the C2 position [46].

Tables S8–S11 in SI summarise the charge transfer (CT) from the pyrazinium-3-olates **1a–d** to the MA **2** and MMA **3** fragment at the TSs of the 13DCs. The CTs are in the range 0.10 e to 0.22 e indicating that these 13DCs have some polar nature. The CT is slightly higher for the *exo* TSs compared to the *endo* ones for the 13DCs of **1a–d** to MA **2** while reaction with MMA **3** results in comparable CT values for the *exo* and *endo* regiosiomers. From these data

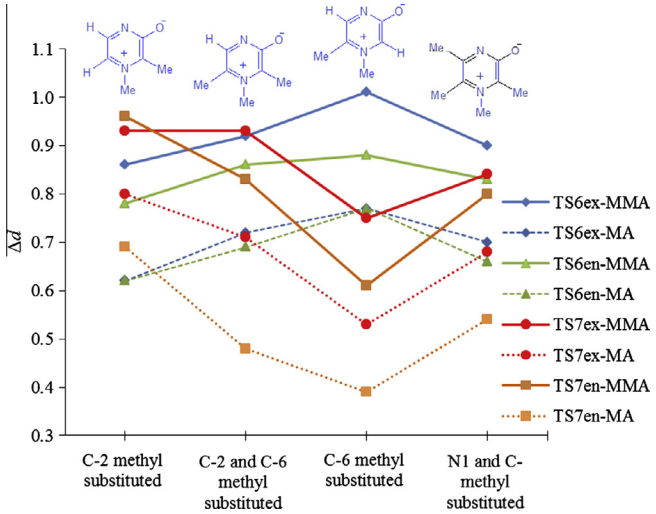

Fig. 4. Degree of asynchronicity, Δd, at the TSs arising from the 13DCs of different C-methyl substituted pyrazinium-3-olates with MA **2** and MMA **3**.

(Tables S8–S11), we also find that CT is higher in the more asynchronous processes whereas TSs formed by less asynchronous sequences have lower values of the CT. The dipole moments of the TSs are also tabulated (see Tables S8–S11 in SI). The greater polar character of the *endo* TSs than the *exo* ones, measured by the dipole moments, accounts for the higher solvation of the former. However, the dipole moments for the 7-esters TSs for the 13DCs of **1c** with MA **2** and MMA **3** are similar.

Table 3
Wiberg bond orders of the TSs involved during the cycloaddition of **1a–d** with MA **2** and MMA **3**.

	1a		**1b**		**1c**		**1d**	
1a–d + MA **2**								
	C2–C6	C3–C2	C2–C6	C3–C2	C2–C6	C3–C2	C2–C6	C3–C2
TS6en	0.14	0.49	0.18	0.51	0.14	0.51	0.16	0.49
TS6ex	0.12	0.48	0.17	0.52	0.13	0.51	0.14	0.50
	C2–C2	C3–C6	C2–C2	C3–C6	C2–C2	C3–C6	C2–C2	C3–C6
TS7en	0.27	0.47	0.18	0.51	0.24	0.50	0.21	0.50
TS7ex	0.22	0.51	0.14	0.51	0.17	0.53	0.17	0.51
1a–d + MMA **3**								
	C2–C6	C3–C2	C2–C6	C3–C2	C2–C6	C3–C2	C2–C6	C3–C2
TS6en	0.12	0.52	0.16	0.55	0.12	0.54	0.14	0.53
TS6ex	0.10	0.50	0.13	0.55	0.10	0.53	0.11	0.52
	C2–C2	C3–C6	C2–C2	C3–C6	C2–C2	C3–C6	C2–C2	C3–C6
TS7en	0.22	0.53	0.14	0.55	0.17	0.57	0.17	0.55
TS7ex	0.18	0.56	0.13	0.53	0.14	0.56	0.14	0.54

Table 4
Electronic chemical potential μ, chemical hardness η, global electrophilicity ω, and global nucleophilicity N indices, in eV, of methyl pyrazinium-3-olates **1a–d**, MA **2** and MMA **3**.

	μ	η	ω	N
1a	−3.48	3.69	1.64	3.80
1b	−3.48	3.74	1.62	3.77
1c	−3.47	3.59	1.68	3.86
1d	−3.35	3.62	1.55	3.96
2	−4.31	6.22	1.49	1.70
3	−4.11	6.22	1.36	1.90

3.4. Analysis based on the reactivity indices at the ground state of reagents

Recent studies devoted to Diels–Alder and 13DC reactions have shown that the analysis of the global and local indices defined within the context of the conceptual DFT [4] are a powerful tool to understand the reactivity in polar cycloadditions. In Table 4, the static global properties, namely electronic chemical potential μ, chemical hardness η, global electrophilicity ω, and global nucleophilicity N indices of methyl pyrazinium-3-olates **1a–d**, MA **2** and MMA **3** are reported, while the local electrophilicity ω_k and local nucleophilicity N_k indices are given in Table 5.

The electronic chemical potentials of MA **2** and MMA **3**, $\mu = -4.31$ and -4.11 eV, respectively, are lower than those of methyl pyrazinium-3-olates **1a–d**, μ are in the range -3.35 to -3.48 eV, indicating that along a polar cycloaddition reaction the net CT will take place from methyl pyrazinium-3-olates **1a–d** towards the electron-deficient MA **2** and MMA **3**, in clear agreement with the CT analysis performed at the TSs.

The electrophilicity indices of methyl pyrazinium-3-olate **1a–d** are in the range 1.55–1.68 eV, which are considered as strong electrophiles based on the electrophilicity scale [47]. On the other hand, methyl pyrazinium-3-olates **1a–d** have high nucleophilicity indices, N, in the range 3.77–3.96 eV, being classified as a strong nucleophiles on the nucleophilicity scale [48]. Note that the tetramethyl derivative **1d** is the most nucleophilic species of this series, $N = 3.96$ eV.

MA **2** and MMA **3** have electrophilicity indices of $\omega = 1.49$ and 1.36 eV, and a nucleophilicity index of $N = 1.70$ and 1.90 eV, respectively, being classified as moderate electrophiles and as moderate nucleophiles. The presence of an electron-releasing methyl group in MMA **3** decreases its electrophilicity slightly and increases its nucleophilicity slightly when compared with MA **2**.

In spite of the fact that methyl pyrazinium-3-olates **1a** and **b** are slightly more electrophilic than MA **2** and MMA **3**, analysis of the electronic chemical potential μ, indicates that the CT will take place from **1a** and **b** to MA **2** and MMA **3**; thus, methyl pyrazinium-3-olates **1a–d** will behave as a nucleophiles, and MA **2** and MMA **3** as electrophiles. This behaviour is reasonable considering the strongly nucleophilic character of methyl pyrazinium-3-olates **1a–d**.

Studies devoted to cycloaddition reactions with a polar character have shown that the analysis of the local electrophilicity index ω_k in the electrophilic component and the local nucleophilicity index N_k in the nucleophilic partner explains the observed regioselectivity [46,49]. In this way, the N_k in methyl pyrazinium-3-olates **1a–d** and the ω_k in MA **2** and MMA **3** were analysed in order to predict the best electrophilic/nucleophilic interaction along a polar cycloaddition path, and thus explain the observed regioselectivity. The corresponding local indices are given in Table 5.

MA **2** and MMA **3** have the largest electrophilic activation at the β conjugated C3 position, $\omega_{C3} = 0.86$ and 0.76 eV, respectively. Note that this position is twice as electrophilically activated as the ester C1 carbon, $\omega_{C1} = 0.37$ and 0.35 eV. The presence of the electron-releasing methyl group at the C2 position of MMA **3** decreases slightly the local electrophilicity at the C3 position when it is compared with that at the C3 position of MA **2**.

For methyl pyrazinium-3-olates **1a–d**, the C2, N4 and C6 positions are nucleophilically activated, while the N1, C3 and C5 position are nucleophilically deactivated; note that the local nucleophilicity indices N_k at these positions present negative values as a consequence of the negative values of the corresponding nucleophilic Parr functions P_k^- (see Table 5). The most nucleophilic centres of the pyrazinium ring of methyl pyrazinium-3-olates **1a–d**, are the C2 carbon, N_{C2} ranges from 1.17 to 1.49 eV, and the C6 carbon, N_{C6} ranges from 1.45 to 1.72 eV. For methyl pyrazinium-3-olates **1b–d**, the C6 position is more nucleophilically activated than the C2 one, indicating that in a polar 13DC reaction involving these methyl pyrazinium-3-olates the preferred site to form the first C–C single bond will be the C6 carbon. However, unfavourable interactions between the carboxylate group of MA **2** and MMA **3** and the anionic oxygen or the C2 methyl group present in pyrazinium-3-olates **1b–d**, which appear along the nucleophilic attack on C6, can be responsible for the change in the observed regioselectivity. Note that while along the 7-regiosiomeric channels the carboxylate group is positioned over the anionic oxygen or the C2 methyl group, along the most favourable 6-regiosiomeric channels they are far (see Figs. 2 and 3).

Finally, the O7 oxygen atom of these methyl pyrazinium-3-olates is also nucleophilically activated, N_{O7} ranges from 1.63 to 1.75 eV. However, the reaction channels involving the nucleophilic approach of the O7 oxygen atom cannot progress, and consequently this interaction reversibly gives the separated original

Table 5
Electrophilic Parr functions, P_k^+, and local electrophilicities, ω_k in eV, of MA **2** and MMA **3**, and nucleophilic Parr functions, P_k^-, and local nucleophilicities, N_k in eV, of pyrazinium-3-olates **1a–d**.

	MA **2**		MMA **3**	
	P_k^+	ω_k	P_k^+	ω_k
O	0.14	0.21	0.15	0.20
C1	0.25	0.37	0.26	0.35
C2	0.08	0.11	0.07	0.10
C3	0.58	0.86	0.56	0.76

	1a		**1b**		**1c**		**1d**	
	P_k^-	N_k	P_k^-	N_k	P_k^-	N_k	P_k^-	N_k
N1	−0.13	−0.51	−0.13	−0.49	−0.13	−0.48	−0.13	−0.51
C2	0.39	1.49	0.31	1.17	0.32	1.23	0.33	1.32
C3	−0.16	−0.61	−0.15	−0.57	−0.15	−0.57	−0.14	−0.57
N4	0.20	0.74	0.24	0.89	0.23	0.88	0.20	0.79
C5	−0.13	−0.48	−0.14	−0.53	−0.13	−0.49	−0.12	−0.47
C6	0.38	1.45	0.46	1.74	0.39	1.50	0.41	1.62
O	0.46	1.75	0.43	1.63	0.44	1.70	0.43	1.71

reactants. On the other hand, the nucleophilic approach of the C2 or C6 positions towards the β conjugated C3 position of MA **2** or MMA **3** can be assisted by the concomitant ring closure with formation of the second C–C bond, to result in the formation of the final [3+2] CAs.

4. Conclusions

The 13DC reactions of multi methyl C-substituted pyrazinium-3-olates with MA **2** and MMA **3** have been studied in the gas phase and THF using DFT methods at the B3LYP/6-31G(d) level. The two possible regioisomeric pathways, forming 6-esters and 7-esters, along with the two stereoisomeric channels, *endo* and *exo*, have been analysed based on the kinetic and thermodynamic parameters, while the regioselectivity has been interpreted using reactivity indices. In all cases, the reaction pathways leading to the *exo* CAs are the favourable ones. These 13DCs take place through a one-step mechanism, *via* asynchronous TSs. The skeleton rearrangement of the 6-*exo* [3+2] CAs into the [4+2] CAs was also considered and concluded to be solvent dependent. Although these rearrangements are kinetically favourable in THF, formation of the corresponding [4+2] CAs are thermodynamically unfavourable. The findings of this theoretical research have been compared with the 13DCs of the previously reported substituted pyrazinium-3-olates with MA **2** and MMA **3**. Furthermore, the recently proposed electrophilic, P_k^+, and nucleophilic, P_k^-, Parr functions indicates that for methyl pyrazinium-3-olates **1b–d** the most favorable regioisomeric reaction channels should be those associated with the approach of the C6 carbon atom of methyl pyrazinium-3-olates **1b–d** towards the β conjugated C3 position of MA **2** or MMA **3**. However, unfavourable interactions between the carboxylate group of MA **2** and MMA **3** and the anionic oxygen or the C2 methyl substituent present in pyrazinium-3-olates **1b–d**, which appear along the nucleophilic attack on C6, can be responsible for the change in observed regioselectivity. We hope that these results and our previous observations should be helpful to experimentalists in planning syntheses involving 13-DCs of pyrazinium-3-olates.

Acknowledgements

Facilities from the University of Mauritius are acknowledged. This work was supported by funding provided by the Tertiary Education Commission (TEC) of Mauritius.

Appendix A. Supplementary material

Supplementary data associated with this article can be found, in the online version, at http://dx.doi.org/10.1016/j.comptc.2013.09.029.

References

[1] A. Padwa, W.H. Pearson (Eds.), Synthetic Applications of 1,3-Dipolar Cycloaddition Chemistry Toward Heterocycles and Natural Products, Wiley and Sons, Hoboken, New Jersey, 2003.
[2] R. Huisgen, 1,3-Dipolar cycloadditions. Past and future, Angew. Chem. Int. Ed. Engl. 2 (1963) 565–598.
[3] A. Padwa, 1,3-Dipolar Cycloaddition Chemistry, vols. 1–2, Wiley Interscience, New York, 1984.
[4] (a) P. Geerlings, F. De Proft, W. Langenaeker, Conceptual density functional theory, Chem. Rev. 103 (2003) 1783–1793;
(b) D.H. Ess, G.O. Jones, K.N. Houk, Conceptual, qualitative and quantitative theories of 1,3-dipolar and Diels–Alder cycloadditions used in synthesis, Adv. Synth. Catal. 348 (2006) 2337–2361.
[5] L.R. Domingo, P. Pérez, J.A. Sáez, Understanding the local reactivity in polar organic reactions through electrophilic and nucleophilic Parr functions, RSC Adv. 3 (2013) 1486–1494.
[6] L. Rhyman, H.H. Abdallah, S. Jhaumeer-Laulloo, L.R. Domingo, J.A. Joule, P. Ramasami, The 1,3-dipolar cycloaddition of 1H-pyridinium-3-olate and 1-methylpyridinium-3-olate with methyl acrylate: a density functional theory study, Tetrahedron 66 (2010) 9187–9193.
[7] L. Rhyman, H.H. Abdallah, S. Jhaumeer-Laulloo, L.R. Domingo, J.A. Joule, P. Ramasami, 1,3-Dipolar cycloaddition of 1H-pyrazinium-3-olate and N1- and C-methyl substituted pyrazinium-3-olates with methyl acrylate: a density functional theory study, Tetrahedron 67 (2011) 8383–8391.
[8] N. Dennis, A.R. Katritzky, Y. Takeuchi, Synthetic applications of heteroaromatic betaines with six-membered rings, Angew. Chem. Int. Ed. Engl. 15 (1976) 1–9.
[9] G. Guiheneuf, C. Laurence, A.R. Katritzky, 1,3-Dipolar character of six-membered aromatic rings: Part XXIX. Kinetic rates and equilibria for the addition of 2π-electron addends to 3-oxidopyridinium betaines, J. Chem. Soc., Perkin Trans. 2 (1976) 1829–1831.
[10] A.P. Kozikowski, G.L. Araldi, R.G. Ball, Dipolar cycloaddition route to diverse analogues of cocaine: the 6- and 7-substituted 3-phenyltropanes, J. Org. Chem. 62 (1997) 503–509.
[11] F. Estour, S. Rézel, D. Fraisse, J. Métin, V. Gaumet, C. Lartigue, G. Miscoria, A. Gueiffier, Y. Blache, J.C. Teulade, O. Chavignon, Regioselectivity of 1,3-dipolar cycloaddition of 3-oxidopyridinium betaines to olefins and stereoselective synthesis of 6-alkyloxy-5-oxa-9-azatricyclo[5.2.1.04,8]decan-2-one derivatives, Heterocycles 50 (1999) 929–945.
[12] L. Rhyman, H.H. Abdallah, S. Jhaumeer-Laulloo, L.R. Domingo, J.A. Joule, P. Ramasami, Regio- and stereoselectivity of the 1,3-dipolar cycloaddition of pyridinium-3-olates and pyrazinium-3-olates with methyl methacrylate: a density functional theory exploration, Curr. Org. Chem. 16 (2012) 1711–1722.
[13] M. Helliwell, Y. You, J.A. Joule, The dipolar cycloaddition of methyl acrylate to 1,5,6-trimethyl-3-oxidopyrazinium, Acta Crystallogr. Sect. E: Struct. Rep. Online 62 (2006) o1293–o1294.
[14] M. Helliwell, Y. You, J.A. Joule, The dipolar cycloaddition of methyl acrylate to 5,6-diethyl-1-methyl-3-oxidopyrazinium, Acta Crystallogr. Sect. E: Struct. Rep. Online 62 (2006) o2318–o2320.
[15] M. Helliwell, Y. You, J.A. Joule, The 1,3-dipolar cycloaddition of methyl acrylate to hindered 3-oxidopyraziniums, Heterocycles 70 (2006) 87–91.

[16] Z. Joomun, J. Raftery, K. Delawarally, S. Jhaumeer-Laulloo, J.A. Joule, 3-Oxidopyraziniums – [4+2] versus [3+2] cycloadditions, Arkivoc xvi (2007) 51–57.
[17] L.R. Domingo, J.A. Sáez, J.A. Joule, L. Rhyman, P. Ramasami, A DFT study of the [3+2] versus [4+2] cycloaddition reactions of 1,5,6-trimethylpyrazinium-3-olate with methyl methacrylate, J. Org. Chem. 78 (2013) 1621–1629.
[18] A.D. Becke, Density-functional exchange-energy approximation with correct asymptotic behavior, Phys. Rev. A 38 (1988) 3098–3100.
[19] C. Lee, W. Yang, R.G. Parr, Development of the Colle–Salvetti correlation-energy formula into a functional of the electron density, Phys. Rev. B 37 (1988) 785–789.
[20] W.J. Hehre, L. Radom, P.v.R. Schleyer, J.A. Pople, Ab Initio Molecular Orbital Theory; Wiley and Sons, New York, 1986.
[21] E. Goldstein, B. Beno, K.N. Houk, Density functional theory prediction of the relative energies and isotope effects for the concerted and stepwise mechanisms of the Diels–Alder reaction of butadiene and ethylene, J. Am. Chem. Soc. 118 (1996) 6036–6043.
[22] L.R. Domingo, M. Arnó, J. Andrés, Toward an understanding of molecular mechanism of domino cycloadditions. Density functional theory study of the reaction between hexafluorobut-2-yne and n, n′-dipyrrolylmethane, J. Am. Chem. Soc. 120 (1998) 1617–1618.
[23] CYLview, 1.0b Legault, C.Y. *Univeristé de Sherbrooke*, 2009 http://www.cylview.org/Home.html.
[24] M.T. Cancès, V. Mennunci, J. Tomasi, A new integral equation formalism for the polarizable continuum model: theoretical background and applications to isotropic and anisotropic dielectrics, J. Chem. Phys. 107 (1997) 3032–3042.
[25] M. Cossi, V. Barone, R. Cammi, J. Tomasi, Ab initio study of solvated molecules: a new implementation of the polarizable continuum model, Chem. Phys. Lett. 255 (1996) 327–335.
[26] V. Barone, M. Cossi, J. Tomasi, Geometry optimization of molecular structures in solution by the polarizable continuum model, J. Comput. Chem. 19 (1998) 404–417.
[27] J. Tomasi, M. Persico, Molecular interactions in solution: an overview of methods based on continuous distributions of the solvent, Chem. Rev. 94 (1994) 2027–2094.
[28] B.Y. Simkin, I. Sheikhet, Quantum Chemical and Statistical Theory of Solutions – A Computational Approach, Ellis Horwood, London, 1995.
[29] A.P. Scott, L. Radom, Harmonic vibrational frequencies: an evaluation of Hartree–Fock, Møller–Plesset, quadratic configuration interaction, density functional theory, and semiempirical scale factors, J. Phys. Chem. 100 (1996) 16502–16513.
[30] K. Fukui, Formulation of the reaction coordinate, J. Phys. Chem. 74 (1970) 4161–4163.
[31] C. Gonzalez, H.B. Schlegel, An improved algorithm for reaction path following, J. Chem. Phys. 90 (1989) 2154–2161.
[32] C. Gonzalez, H.B. Schlegel, Reaction path following in mass-weighted internal coordinates, J. Phys. Chem. 94 (1990) 5523–5527.
[33] A.E. Reed, R.B. Weinstock, F. Weinhold, Natural population analysis, J. Chem. Phys. 83 (1985) 735–747.
[34] A.E. Reed, L.A. Curtiss, F. Weinhold, Intermolecular interactions from a natural bond orbital, donor-acceptor viewpoint, Chem. Rev. 88 (1988) 899–926.
[35] Gaussian 09, Revision A.1, M.J. Frisch, G.W. Trucks, H.B. Schlegel, G.E. Scuseria, M.A. Robb, J.R. Cheeseman, G. Scalmani, V. Barone, B. Mennucci, G.A. Petersson, H. Nakatsuji, M. Caricato, X. Li, H.P. Hratchian, A.F. Izmaylov, J. Bloino, G. Zheng, J.L. Sonnenberg, M. Hada, M. Ehara, K. Toyota, R. Fukuda, J. Hasegawa, M. Ishida, T. Nakajima, Y. Honda, O. Kitao, H. Nakai, T. Vreven, J. A. Montgomery, Jr., J.E. Peralta, F. Ogliaro, M. Bearpark, J.J. Heyd, E. Brothers, K.N. Kudin, V.N. Staroverov, R.Kobayashi, J. Normand, K. Raghavachari, A. Rendell, J.C. Burant, S.S. Iyengar, J. Tomasi, M. Cossi, N. Rega, J.M. Millam, M. Klene, J.E. Knox, J.B. Cross, V. Bakken, C. Adamo, J. Jaramillo, R. Gomperts, R. E. Stratmann, O. Yazyev, A.J. Austin, R. Cammi, C. Pomelli, J.W. Ochterski, R.L. Martin, K. Morokuma, V.G. Zakrzewski, G.A. Voth, P. Salvador, J.J. Dannenberg, S. Dapprich, A.D. Daniels, Ö. Farkas, J.B. Foresman, J.V. Ortiz, J. Cioslowski, and D.J. Fox, Gaussian Inc., Wallingford CT, 2009.
[36] R.G. Parr, L. von Szentpaly, S. Liu, Electrophilicity index, J. Am. Chem. Soc. 121 (1999) 1922–1924.
[37] R.G. Parr, R.G. Pearson, Absolute hardness: companion parameter to absolute electronegativity, J. Am. Chem. Soc. 105 (1983) 7512–7516.
[38] R.G. Parr, W. Yang, Density Functional Theory of Atoms and Molecules, Oxford University, New York, 1989.
[39] W. Kohn, L. Sham, Self-consistent equations including exchange and correlation effects, J. Phys. Rev. 140 (1965) A1133–A1135.
[40] L.R. Domingo, E. Chamorro, P. Pérez, Understanding the reactivity of captodative ethylenes in polar cycloaddition reactions. A theoretical study, J. Org. Chem. 72 (2008) 4615–4624.
[41] L.R. Domingo, P. Pérez, The nucleophilicity N index in organic chemistry, Org. Biomol. Chem. 9 (2011) 7168–7175.
[42] L.R. Domingo, M.J. Aurell, P. Pérez, R. Contreras, Quantitative characterization of the local electrophilicity of organic molecules. Understanding the regioselectivity on Diels–Alder reactions, J. Phys. Chem. A 106 (2002) 6871–6875.
[43] P. Pérez, L.R. Domingo, M. Duque-Noreña, E. Chamorro, A condensed-to-atom nucleophilicity index. An application to the director effects on the electrophilic aromatic substitutions, J. Mol. Struct. (Theochem) 895 (2009) 86–91.
[44] W. Benchouk, S.M. Mekelleche, B. Silvi, M.J. Aurell, L.R. Domingo, Understanding the kinetic solvent effects on the 1,3-dipolar cycloaddition of benzonitrile N-oxide: a DFT study, J. Phys. Org. Chem. 24 (2011) 611–618.
[45] K.B. Wiberg, Application of the pople-santry-segal CNDO method to the cyclopropylcarbinyl and cyclobutyl cation and to bicyclobutane, Tetrahedron 24 (1968) 1083–1096.
[46] M.J. Aurell, L.R. Domingo, P. Pérez, R. Contreras, A theoretical study on the regioselectivity of 1,3-dipolar cycloadditions using DFT-based reactivity indexes, Tetrahedron 60 (2004) 11503–11509.
[47] L.R. Domingo, M.J. Aurell, P. Pérez, R. Contreras, Quantitative characterization of the global electrophilicity power of common dienedienophile pairs in Diels–Alder reactions, Tetrahedron 58 (2002) 4417–4423.
[48] P. Jaramillo, L.R. Domingo, E. Chamorro, P. Pérez, A further exploration of a nucleophilicity index based on the gas-phase ionization potentials, J. Mol. Struct. (Theochem) 865 (2008) 68–76.
[49] (a) P. Pérez, L.R. Domingo, M.J. Aurell, R. Contreras, Quantitative characterization of the global electrophilicity pattern of some reagents involved in 1,3-dipolar cycloaddition reactions, Tetrahedron 59 (2003) 3117–3125;
(b) P. Pérez, L.R. Domingo, A. Aizman, R. Contreras, Theoretical Aspects of Chemiscal Reactivity: Toro-Labbé, A., Ed.; Elsevier Science, Amsterdam, The Netherlands, vol. 19, 2007, pp 139–201.;
(c) L.R. Domingo, M.J. Aurell, P. Pérez, J.A. Sáez, Understanding the origin of the asynchronicity in bond-formation in polar cycloaddition reactions. A DFT study of the 1,3-dipolar cycloaddition reaction of carbonyl ylides with 1,2-benzoquinones, RSC Adv. 2 (2012) 1334–1342.